Materials Science Forum Vols. 727-728 (2012) pp 904-908
Online available since 2012/Aug/24 at www.scientific.net

doi:10.4028/www.scientific.net/MSF.727-728.904

Synthesis and characterization of strontium and calcium titanate polycrystalline powders by a modified polymeric precursor technique

R. Muccillo[a], J. R. Carmo[b]

[1]Center of Science and Technology of Materials, Energy and Nuclear Research Institute, Travessa R 400, Cidade Universitaria, S. Paulo, SP, Brazil

[a]muccillo@usp.br, [b]jrcarmo@gmail.com

Keywords: strontium titanate, calcium titanate, chemical synthesis, thermal analysis.

Abstract. $SrTi_{0,65}Fe_{0,35}O_{3-\delta}$, $Ca_{0,5}Sr_{0,5}Ti_{0,65}Fe_{0,35}O_{3-\delta}$, $CaTi_{0,65}Fe_{0,35}O_{3-\delta}$ ceramic powders were synthesized by the polymeric precursor technique using $CaCO_3$, $SrCO_3$, $C_{12}H_{28}O_4Ti$ and $Fe(NO_3)_{3.9}H_2O$. After calcination, each powder was heat treated at temperatures chosen according to data collected on thermogravimetric-differential thermal analysis experiments. The compositions were analyzed by X-ray diffraction for structural phase evaluation (either perovskite cubic or orthorhombic), laser scattering for determination of particle size distribution and average particle size, transmission electron microscopy (TEM) for observation of particle shape and average true size. Pressed powders sintered at 1250°C were analyzed by X-ray diffraction and X-ray fluorescence; their surfaces were observed by scanning probe microscopy (SPM) for topographical analysis of grains and grain boundaries. TEM results show that the powders consist of agglomerated nanoparticles. Sr-based compounds have cubic perovskite phases whereas Ca-based compounds are orthorhombic. SPM images show intergranular features which might be responsible for reported blocking of charge carriers observed in impedance spectroscopy diagrams.

Introduction

$SrTiO_3$ (STO) compound are ceramic materials with thermoelectric behavior. The STO-based oxides are a promising group of *n*-type thermoelectric materials because they exhibit excellent electronic transport properties and are basically stable at high temperatures [1]. Cation aliovalent substitution for strontium leads to compounds with different interesting properties either in bulk ceramic or thin/thick film specimens. Recently, several studies on $SrTi_{1-x}Fe_xO_{3-\delta}$ (STFO) compounds were undertaken looking for suitable compositions for use in temperature independent oxygen automotive lambda sensors [2-9]. These compounds exhibit mixed ionic-electronic conductivity at elevated temperatures (> 550 °C), predominant *n*-type electronic conductivity at low oxygen pressures, ionic conductivity at intermediate oxygen pressures, and *p*-type electronic conductivity at high oxygen pressures, and the oxygen vacancy concentration is found to be independent on the partial pressure of oxygen [5]. Fe ions are considered to be one of the main constituents of the $SrTi_{0.65}Fe_{0.35}O_{3-\delta}$ compound and not just an acceptor impurity dopant with such a high level [5]. Moreover, the composition $SrTi_{0.65}Fe_{0.35}O_{3-\delta}$, in which 0.35 mol of Ti is replaced by Fe, shows a zero temperature coefficient of resistance (zero-TCR), i.e., the electrical response depends only on the partial pressure of oxygen in a certain temperature range, being consequently the optimized composition for a temperature independent oxygen sensor [2,3]. For this reason measurements on compositions with 0.35 mol Fe are here reported. Recent applications of strontium titanate based materials have also been reported on application as anode in solid oxide fuel cell devices due to their electrical behavior and the mechanical compatibility with the yttria-stabilized zirconia solid electrolyte [10,11]. $CaTiO_3$ (CTO), which has a distorted perovskite structure with orthorhombic symmetry at room temperature, shows also the ability of forming solid solutions with a large number of oxides and, therefore, many compounds have been synthesized for different applications [12-18].

Here a careful examination was pursued on the chemical synthesis, thermal and structural analyses of $SrTi_{0.65}Fe_{0.35}O_{3-\delta}$, $CaTi_{0.65}Fe_{0.35}O_{3-\delta}$ and $Ca_{0.5}Sr_{0.5}Ti_{0.65}Fe_{0.35}O_{3-\delta}$ synthesized by the polymeric precursor technique.

Experimental

$Ca_{1-x}Sr_xTi_{0.65}Fe_{0.35}O_{3-\delta}$, x= 0, 0.5 and 1 (hereafter CTFO, CSTFO and STFO), powders were prepared according to the polymeric precursor technique, consisting of mixing under stirring at 100 °C stoichiometric amounts of calcium carbonate ($CaCO_3$), strontium carbonate ($SrCO_3$), iron nitrate ($Fe(NO_3)_3.9H_2O$) and titanium isopropoxide ($C_{12}H_{28}O_4Ti$) (all from Alfa Aesar), in an acid solution (H_2O/HNO_3=20/1); after stirring for 20 min, citric acid and ethylene glycol were added stepwise to the solution under stirring for 30 min, yielding a highly viscous resin, which had the organics burnt out after calcination at 200, 250 and 300 °C for 2 h and at 800 °C for 5 h. These temperature profiles were chosen after evaluating the thermogravimetric analysis of the resins. Simultaneous thermogravimetry and differential thermal analyses were carried out in a Netzsch STA409E equipment in room temperature-1250°C-room temperature cycle, both under flowing 10 mL/min synthetic air. Approximately 60 mg of the viscous resin were glued inside the alumina crucible. Dried alpha-alumina was always used as reference inside a similar alumina crucible. The thermogravimetry and differential thermal analysis data were processed with the Netzsch Proteus® software allowing for evaluating onset and peak temperatures, peak areas, mass loss/gain, etc., besides smoothing noisy raw data.

X-ray diffraction experiments were carried out in all compositions in a Bruker-AXS D8 Advance X-ray diffractometer with θ-2θ Bragg-Brentano configuration with Cukα radiation with Ni filter, 40 kV-40 mA, in the 10-90° 2θ range, 0.05° step size, and 5 s counting time per step. The powders of each composition, namely, STFO, CTFO and CSTFO were pressed to 12 mm diameter disks (uniaxially at 96 MPa, followed by isostatically at 210 MPa). Sintering was performed in air in a programmable furnace at 1300 °C for 2 h, 5 °C/min heating and cooling rates. Suspensions of the calcined powders were observed in a transmission electron microscope Jeol 2100. The polished surfaces of the sintered pellets were observed in a scanning probe microscope (Jeol JSPM-5200, contact mode, dynamic force topography images, 10 μm x 10 μm scanning area). After polishing, the specimens were thermally etched at 1200 °C/20 min.

Results

The results of the thermal analysis experiments, Fig. 1, from 25 to 1550 ^oC under synthetic air flow (5 mL/min) of the $SrTi_{0.65}Fe_{0.35}O_{3-\delta}$ powder obtained by calcinations of the polymeric resin at 200, 250 and 300°C for 2 h and at 800°C for 5 h. The total mass loss is 71.8% from 200 to 815 °C. The initial ~5% mass loss is probably due to water and carbon dioxide removal. Both are known to be easily incorporated in strontium titanate during lab handling. The subsequent mass loss up to 815 ^oC corresponds to elimination of organic compounds retained in the samples after the preliminary calcination procedure. In the differential thermal analysis curve (Fig. 1, right), the exothermic peak at 815 ^oC corresponds to the formation of the $SrTi_{0,65}Fe_{0,35}O_{3-\delta}$ crystalline phase. For the $CaTi_{0.65}Fe_{0.35}O_{3-\delta}$ resin, the total mass loss is 65.0% in the temperature range 200-720 ^oC in two steps. The exothermic peak at 700 ^oC is here associated to the crystalline formation of $CaTi_{0.65}Fe_{0.35}O_{3-\delta}$. All DTA curves show four endothermic and one exothermic events at temperatures which depend on the cation located at the A site in the perovskite ABO_3 structure. All TG curves are also similar. For the solid state synthesis the main events are the de composition of the carbonates. For the resins the main events are the loss of adsorbed water, adsorbed carbon dioxide and remaining organics used in the synthesis.

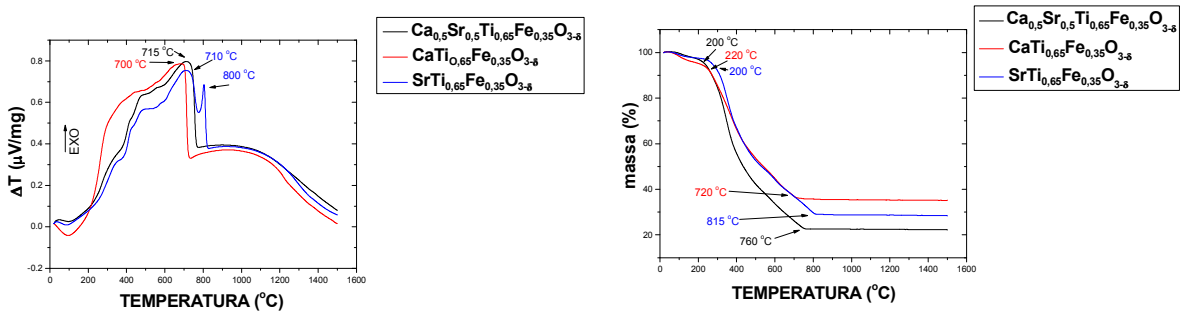

Fig. 1. Differential thermal analysis (left) and thermogravimetric (right) curves of the polymeric resin.

Fig. 2 shows the results of the X-ray diffraction experiments on STFO, CTFO and CSTFO powders.

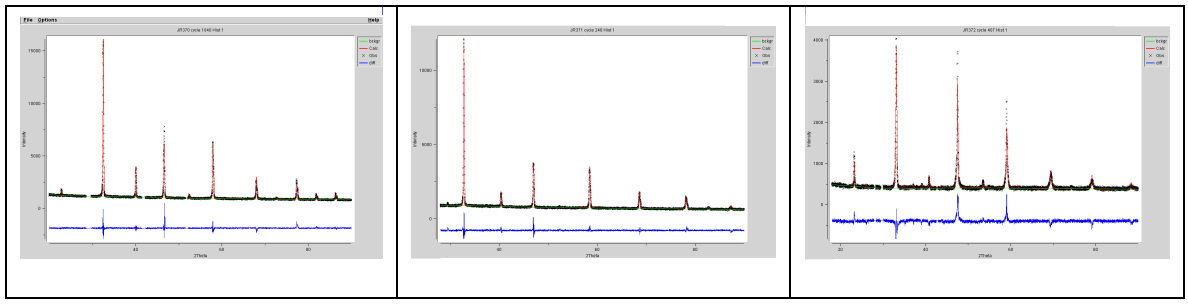

Fig. 2. X-ray diffraction patterns and Rietveld data of $SrTi_{0.65}Fe_{0.35}O_{3-\delta}$ (left), $Ca_{0.5}Sr_{0.5}Ti_{0.65}Fe_{0.35}O_{3-\delta}$ (middle) and $CaTi_{0.65}Fe_{0.35}O_{3-\delta}$ (right) powders.

Rietveld analyses performed with the GSAS software [19] of X-ray diffraction data of the compounds synthesized by the polymeric precursor technique give the following values for the lattice parameters: perovskite orthorhombic with a = 5.41309 (0.00004) Å, b = 7.65496 (0.00006) Å and c = 5.41091 (0.00008) Å for $CaTi_{0.65}Fe_{0.35}O_{3-\delta}$; perovskite orthorhombic with a = 5.47077 (0.00004) Å, b = 5.47163 (0.00005) Å and c = 7.73996 (0.00006) Å for $Ca_{0.5}Sr_{0.5}Ti_{0.65}Fe_{0.35}O_{3-\delta}$; perovskite cubic with a = b = c = 3.90141 (0.00001) Å for $SrTi_{0.65}Fe_{0.35}O_{3-\delta}$. The sharp and single diffraction peaks in the X-ray diffraction patterns of the powders synthesized by the polymeric precursor route show that these powders present single cubic perovskite phase, as expected from a chemical synthesis.

Fig. 3 shows a typical TEM image of the powders obtained after calcination of the polymeric resin. The powders consist of agglomerated nanoparticles with average size less than 20 nm.

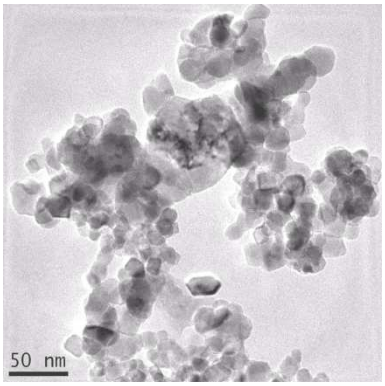

Fig. 4. TEM image of a STFO powder.

Fig. 5 shows topographic images of STFO, SCTFO and CTFO surfaces of sintered pellets, measured in the scanning probe microscope.

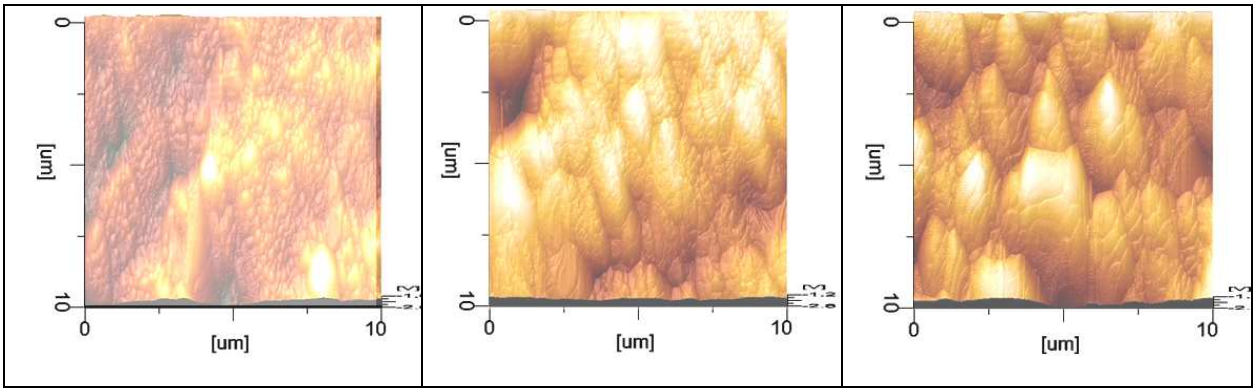

Fig. 5. Scanning probe microscopy topographic images of polished and thermally etched surfaces of $SrTi_{0,65}Fe_{0,35}0_{3-\delta}$ (left) $Ca_{0,5}Sr_{0,5}Ti_{0,65}Fe_{0,35}0_{3-\delta}$ (middle) and $CaTi_{0,65}Fe_{0,35}O_{3-\delta}$ (right) sintered pellets.

The specimens prepared with powders synthesized by the chemical route are highly homogeneous, dense and composed of well defined grains, such that each grain is itself composed of a large number of tightly packed sub-grains.

Conclusions

Powders of $SrTi(Fe)O_3$ (STFO), in $CaTi(Fe)O_3$ (CTFO), and in $Ca_{0.5}Sr_{0.5}Ti(Fe)O_3$ (CSTFO) compounds, synthesized by a chemical route (polymeric precursor technique), show perovskite cubic structure. Sintered pellets prepared with these powders present homogeneous grains and sub-grains.

Acknowledgements: This work was supported by FAPESP (Grants Nos. 95/05172-4, 98/14324-0 and 05/53241-9) and CNPq. The authors thank Dr. L.G. Martinez for the Rietveld analyses, Y.V. França for the thermal analysis and N. Ferreira for the TEM measurements.

References

[1] K. Koumoto, Y. Wang, R. Zhang, A. Kosuga and R. Funahashi, Annu. Rev. Mater. Res. Vol. 40 (2010), p. 363.

[2] W. Menesklou, H.J. Schreiner, K.H. Hardtl and E. Ivers-Tiffée, Sens. Act. B Vol. 59 (1999), p. 184.

[3] E. Ivers-Tiffée, K.H. Hardtl, W. Menesklou and J. Riegel. Electrochim. Acta Vol. 47 (2001), p. 807.

[4] R. Moos, W. Menesklou, H.-J. Schreiner and K.H. Hardtl, Sens. Act. B Vol. 67 (2000), p. 178.

[5] A. Rothschild, W. Menesklou, H.L. Tuller and E. Ivers-Tiffée, Chem. Mater. Vol. 18 (2006), p. 3651.

[6] K. Sahner, J. Straub and R. Moos, J. Electroceram. Vol. 16 (2006), p. 179.

[7] R. Moos, F. Rettig, A. Huerland and C. Plog, Sensor Actuat. B-Chem Vol. 93 (2003), p. 43.

[8] A. Rothschild and H.L. Tuller, J. Electroceram. Vol. 17 (2006), p. 1005.

[9] A. Rothschild, S.J. Litzelman, H.L. Tuller, W. Menesklou, T. Schneider and E. Ivers-Tiffée, Sens. Act. B Vol. 108 (2005), p. 223.

[10] D. Neagu and J.T.S. Irvine, Chem. Mater. Vol. 22 (2010), p. 5042.

[11] P. Blennow, K.K. Hansen, L.R. Wallenberg and M. Mogensen, Advances is Solid Oxide Fuel Cells III, Ceramic Engineering and Science Proc. 28 (2008), p. 203.

[12] Y. Hanajiri, H. Yokoi, T. Matsui, Y. Arita, T. Nagasaki and H. Shigematsu, J. Nucl. Mater. Vol. 247 (1997), p. 285.

[13] Y. Li, S. Qin and F. Seifert, J. Solid State Chem. Vol. 180 (2007), p. 824.

[14] A.G. Andersen, T. Hayakawa, T. Tsunoda, H. Orita, M. Shimizu and K. Takehira, Catal. Lett. Vol. 18 (1993), p. 37.

[15] V.M. Ferreira, F. Azough, J.L. Baptista and R. Freer, J. Mater. Res. Vol. 12 (1997), p. 3293.

[16] E.R. Kipkoech, F. Azough, R. Freer, C. Leach, S.P. Thompson and C.C. Tang, J. Eur. Ceram. Soc. Vol. 23 (2003), p. 2677.

[17] L. Zhou, P.M. Vilarinho and J.L. Baptista, J. Am. Ceram. Soc. Vol. 82 (1999), p. 1064.

[18] K.D. Madal, L. Behera and K. Ismail, J. Alloy Compd. Vol. 325 (2003), p. 309.

[19] A.C. Larson and R.B.V. Dreele, *General Structure Analysis System (GSAS)* (Los Alamos National Laboratory Report LAUR 86-748, 2004).

Advanced Powder Technology VIII
10.4028/www.scientific.net/MSF.727-728

Synthesis and Characterization of Strontium and Calcium Titanate Polycrystalline Powders by a Modified Polymeric Precursor Technique
10.4028/www.scientific.net/MSF.727-728.904